

## Research Paper

# Glypican-3-targeted precision diagnosis of hepatocellular carcinoma on clinical sections with a supramolecular 2D imaging probe

Hai-Hao Han<sup>1\*</sup>, Yu-Jiao Qiu<sup>1\*</sup>, Yuan-Yuan Shi<sup>2\*</sup>, Wen Wen<sup>2</sup>, Xiao-Peng He<sup>1</sup>✉, Li-Wei Dong<sup>2</sup>✉, Ye-Xiong Tan<sup>2</sup>✉, Yi-Tao Long<sup>1</sup>, He Tian<sup>1</sup>, Hong-Yang Wang<sup>2</sup>✉

1. Key Laboratory for Advanced Materials & Feringa Nobel Prize Scientist Joint Research Center, East China University of Science and Technology (ECUST), 130 Meilong Rd., Shanghai 200237, PR China
2. International Cooperation Laboratory on Signal Transduction, Eastern Hepatobiliary Surgery Institute, the Second Military Medical University, Shanghai 200433, PR China

\*These authors contributed equally to this work.

✉ Corresponding authors: xphe@ecust.edu.cn (X.-P. He); donliwei@126.com (L.-W. Dong); yxtan1214@163.com (Y.-X. Tan); hywangk@vip.sina.com (H.-Y. Wang)

© Ivyspring International Publisher. This is an open access article distributed under the terms of the Creative Commons Attribution (CC BY-NC) license (<https://creativecommons.org/licenses/by-nc/4.0/>). See <http://ivyspring.com/terms> for full terms and conditions.

Received: 2018.01.03; Accepted: 2018.03.10; Published: 2018.05.11

## Abstract

The ability of chemical tools to effectively detect malignancy in frozen sections removed from patients during surgery is important for the timely determination of the subsequent surgical program. However, current clinical methods for tissue imaging rely on dye-based staining or antibody-based techniques, which are sluggish and complicated.

**Methods:** Here, we have developed a 2D material-based supramolecular imaging probe for the simple, rapid yet precise diagnosis of hepatocellular carcinoma (HCC). The 2D probe is constructed through supramolecular self-assembly between a water soluble, fluorescent peptide ligand that selectively targets glypican-3 (GPC-3, a specific cell-surface biomarker for HCC) and 2D molybdenum disulfide that acts as a fluorescence quencher as well as imaging enhancer.

**Results:** We show that the 2D imaging probe developed with minimal background fluorescence can sensitively and selectively image cells overexpressing GPC-3 over a range of control cells expressing other membrane proteins. Importantly, we demonstrate that the 2D probe is capable of rapidly (signal became readable within 1 min) imaging HCC tissues over para-carcinoma regions in frozen sections derived from HCC patients; the results are in accordance with those obtained using traditional clinical staining methods.

**Conclusion:** Compared to conventional staining methods, which are laborious (e.g., over 30 min is needed for antibody-based immunosorbent assays) and complex (e.g., diagnosis is based on discrimination of the nucleus morphology of cancer cells from that of normal cells), our probe, with its simplicity and quickness, might become a promising candidate for tumor-section staining as well as fluorescence imaging-guided surgery.

Key words: hepatocellular carcinoma, glypican-3, 2D material, frozen section, diagnostics

## Introduction

Hepatocellular carcinoma (HCC) is the fifth most prevalent malignancy and the second leading cause of cancer-related deaths worldwide. It is estimated that there are more than 782,000 new cases and 746,000

resultant deaths annually [1]. Liver resection is the cornerstone of HCC treatment, and the thorough removal of HCC tissues is vital to improve the overall survival rate of patients [2]. The invasion level of

cancer is assessed pre-operatively with imaging techniques such as magnetic resonant imaging and computed tomography. However, assessment of tumor invasion during operation is crucial for surgeons to precisely remove the malignant tissues. There is always a trade-off between the removal of malignant tissues and preservation of relatively normal structures. As a consequence, intra-operative pathology diagnosis based on effective immunohistochemistry, which largely depends on HCC-specific biomarkers, is crucial for HCC treatment. Effective immunohistochemical methods have been developed mainly as a support technique for the diagnosis of various tumors. However, problems remain in terms of the instability of specimens during the preparation and immunostaining of frozen sections, as well as the long time and complex procedures required for current staining techniques.

Glypican-3 (GPC-3) is a heparan sulfate proteoglycan responsible for regulating embryonal cell growth [3]. GPC-3 is an ideal biomarker for HCC because it is overexpressed in up to 80% of HCC patients, and is absent in normal tissues, cirrhotic liver, and benign lesions [4]. As a membrane-bound proteoglycan, GPC-3 can be easily stained by the antibody-based technique, and the immunohistochemical staining of GPC-3 has demonstrated a 97% specificity for HCC diagnosis [5].

The rise of graphene [6] has led to an ever-growing interest in academia to develop 2D materials for a number of practical applications [7-10]. In recent years, water soluble, biocompatible 2D materials and composites have also been extensively constructed for biomedical applications [11-16]. Among the 2D materials reported, 2D molybdenum disulfide ( $\text{MoS}_2$ ) has been proven to be of low cytotoxicity, good water solubility, and high biocompatibility by several *in vivo* studies [17-19]. They have also been successfully used as a material substrate for fluorogenic biosensing, bioimaging [13, 20-27] and *in vivo* theranostics (e.g., multimodal imaging and photodynamic and photothermal therapy) [28]. Despite the rapidly increasing biomedical studies of 2D materials, their potential in diagnosis of pathological sections has not been fully explored [27].

Here, we developed a 2D imaging probe for the effective diagnosis of frozen sections removed from HCC patients. A fluorophore-tagged peptide ligand for GPC-3 was used for the self-assembly with 2D  $\text{MoS}_2$ , producing a 2D probe with minimal fluorescence and high affinity for GPC-3. This probe has been shown to be capable of 1) imaging HCC cells over a number of control cells without GPC-3

expression and 2) rapidly imaging HCC pathological sections over para-carcinoma tissues.

## Methods

Written informed consent was obtained from patients, and the protocol was approved by the Review Board of the Eastern Hepatobiliary Surgery Hospital. For the complete Methods section, see Supplementary Material.

## Results and discussion

### Construction and characterization of the 2D imaging probe

A known peptide ligand (RLNVGGTYFLTRQ) for GPC-3 [29] was used for the synthesis of the peptide probe. To increase the water solubility, three arginine groups (K) were grafted to the peptide [30], followed by the introduction of 5-TAMRA (5-carboxytetramethylrhodamine) as the fluorescence reporter (**Figure 1A**). Then, the peptide probe (P-probe) dissolved in water was mixed with a homogenous 2D  $\text{MoS}_2$  solution [21] for supramolecular self-assembly, producing the 2D imaging probe (2D probe). A series of techniques were subsequently used for the characterization of the 2D probe. We determined that the morphology of P-probe was particle-like (**Figure 1B**, inset), which might be the result of an amphiphilic self-assembly of the probe possessing three arginine groups. Upon further assembly with 2D  $\text{MoS}_2$ , the peptide particles were observed to be adhered onto the material surface (**Figure 1B**) without interrupting the crystal structure of 2D  $\text{MoS}_2$  (**Figure 1B**, the enlarged areas display the (1 0 0) facet of 2D  $\text{MoS}_2$ , for example) [31]. Adhesion of the spherical aggregates of P-probe to the surface of 2D  $\text{MoS}_2$  was also corroborated by atomic force microscopy (**Figure S1**). Energy dispersive X-ray spectrometry mapping analysis also showed the presence of P-probe on 2D  $\text{MoS}_2$  since additional C, N and O signals belonging to the peptide were observed for the 2D probe (**Figure 1C**).

Next, Raman spectroscopy was used to characterize the assembly between the material and peptide. The increased  $E_{2g}^1$  (~379 nm) /  $A_{1g}$  (~405 nm) ratio of the 2D probe (0.62) with respect to 2D  $\text{MoS}_2$  (0.57) implies a perturbed in-plane motion between S and Mo [32], suggesting the coating of P-probe to the material surface (**Figure 2A**). In addition, the zeta potential of the 2D probe increased with respect to that of the 2D material alone upon assembly with the positively charged TAMRA probe (**Figure 2B**), and dynamic light scattering also showed that the particle size of 2D probe (PDI = 0.301, average size = 534.7 nm) was larger than that of 2D  $\text{MoS}_2$  (PDI = 0.164, average size = 207.0 nm) (**Figure 2C**).

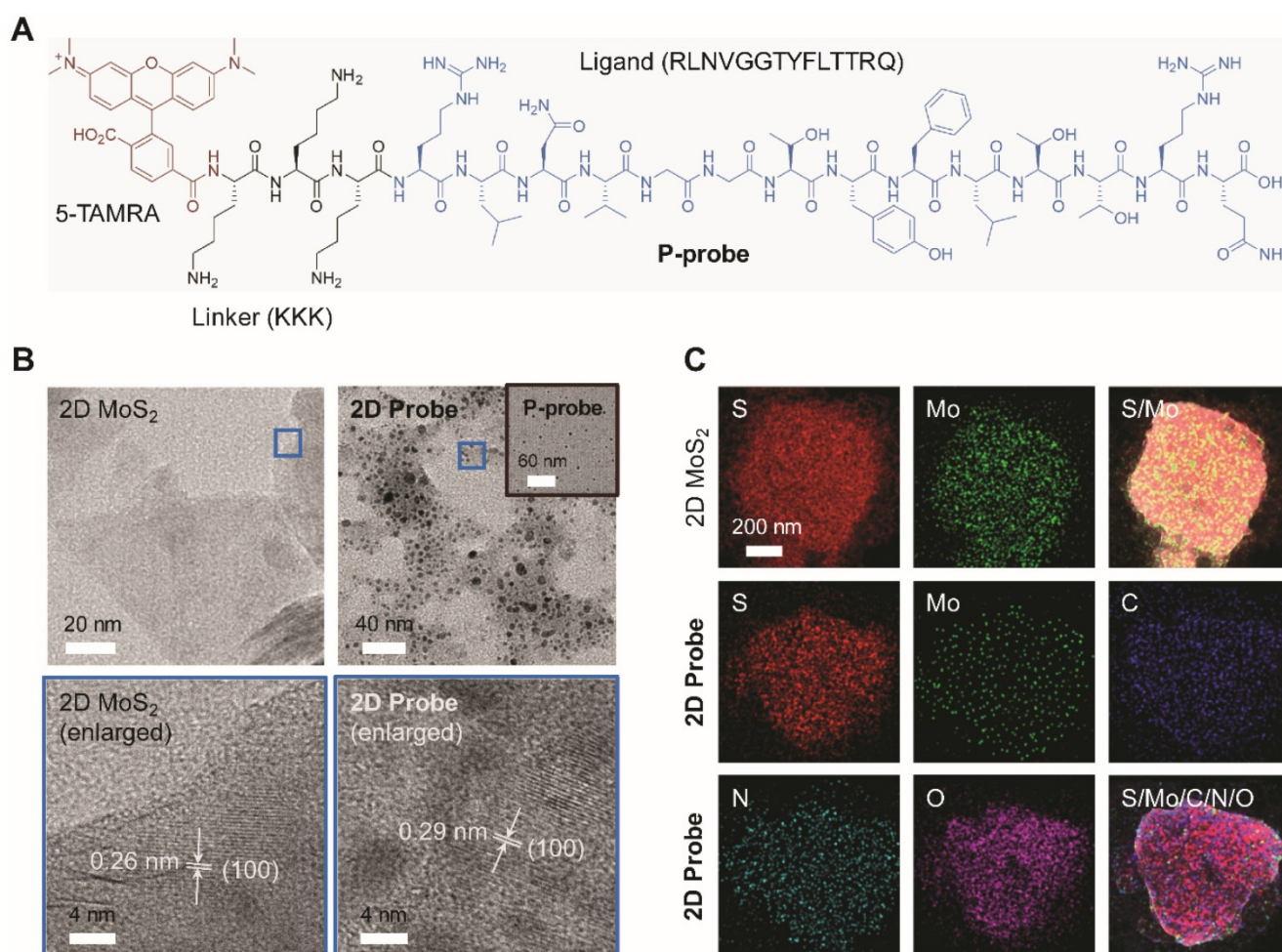


**Figure 1.** (A) Structure of the fluorophore-tagged peptide probe (P-probe) for glypican-3 (GPC-3). (B) High-resolution transmission electron microscopy images of 2D MoS<sub>2</sub>, P-probe (inset) and 2D probe (P-probe/2D MoS<sub>2</sub> = 2 μM/40 μg mL<sup>-1</sup>). The enlarged images show the surface structure of the materials in the blue frames of the images above. (C) Energy dispersive X-ray spectrometry mapping analysis of 2D MoS<sub>2</sub> and 2D probe.

Since it has been reported that 2D MoS<sub>2</sub> can quench the fluorescence of closely attached fluorophores, fluorescence microscopy was used to measure the optical properties of the 2D probe. It was determined that the fluorescence of P-probe was gradually quenched with increasing 2D MoS<sub>2</sub> (Figure 2D), suggesting the assembly between the two species [21, 24, 27]. In a subsequent titration assay, we further determined that the 2D probe showed a gradually enhanced fluorescence with increasing GPC-3 in a homogenous buffer solution (Figure 2E), and the fluorescence was hardly changed in the presence of a range of unselective proteins and ions (Figure 2F). These data suggest that the peptide ligand on the surface of the 2D probe can be removed from the 2D MoS<sub>2</sub> surface because of a selective binding with GPC-3, thereby leading to the enhancement of fluorescence [24, 27]. The subnanomolar limit of detection (0.16 nM) suggests the good sensitivity of the 2D probe for GPC-3, setting the basis for imaging endogenous GPC-3 on the surface of cancer cells.

### GPC-3-targeted imaging of HCC cells

Having successfully constructed the 2D probe, we further tested its ability for GPC-3-targeted cell imaging. A human hepatoma cell line (Hep-G2) was used. In previous studies, we have shown that the presence of 2D materials can drastically enhance the imaging capacity of fluorophore-tagged bioligands probably through the enhancement of the avidity between the ligand and its transmembrane receptor [21, 24, 27]. Therefore, we examined the imaging efficiency of the P-probe with increasing 2D MoS<sub>2</sub>. The result showed that the fluorescence of P-probe was gradually enhanced in Hep-G2 with 2D MoS<sub>2</sub> (Figure 3A, C); with 20 μg mL<sup>-1</sup> of 2D MoS<sub>2</sub>, the fluorescence intensity was almost 7-fold larger than that of P-probe alone (Figure 3C). This suggests that the supramolecular 2D probe could enhance the binding of the peptide probe with GPC-3, which is in agreement with our previous observations [24, 27]. We then used a normal human liver cell line (L02) to test the imaging specificity of the probe.

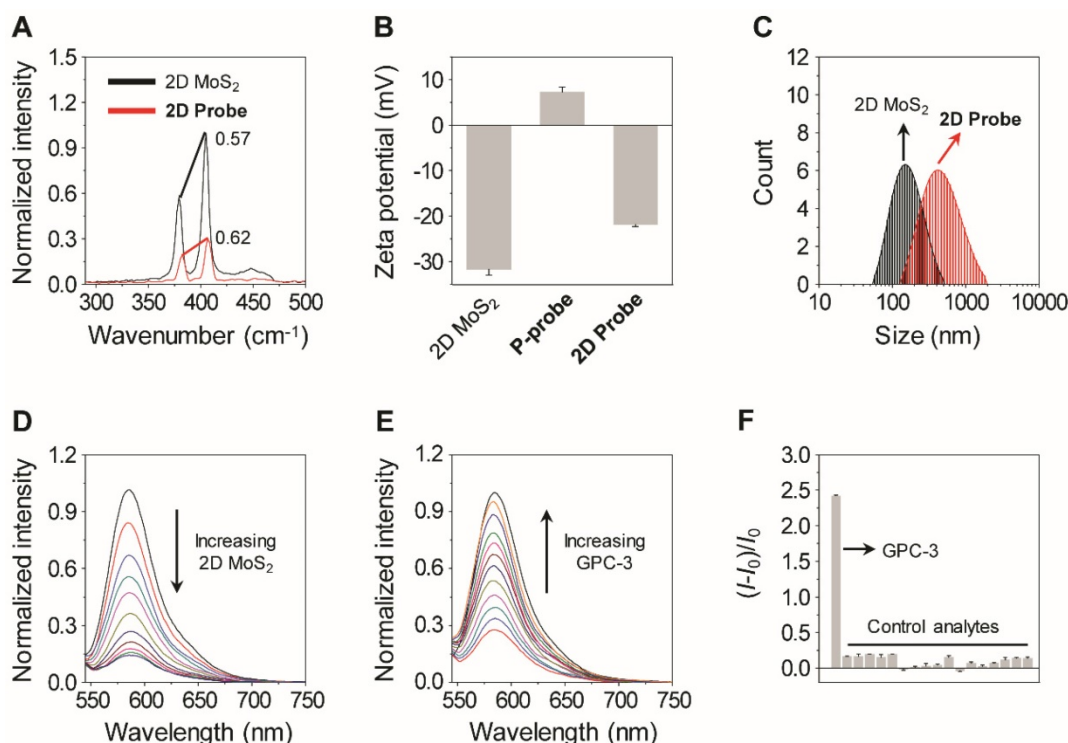


**Figure 2.** (A) Raman spectra of 2D MoS<sub>2</sub> (40 μg mL<sup>-1</sup>) and 2D probe (P-probe/2D MoS<sub>2</sub> = 2 μM/40 μg mL<sup>-1</sup>). (B) Zeta potential of P-probe (2 μM), 2D MoS<sub>2</sub> (40 μg mL<sup>-1</sup>) and 2D probe (P-probe/2D MoS<sub>2</sub> = 2 μM/40 μg mL<sup>-1</sup>). (C) Dynamic light scattering of P-probe (2 μM), 2D MoS<sub>2</sub> (40 μg mL<sup>-1</sup>) and 2D probe (P-probe/2D MoS<sub>2</sub> = 2 μM/40 μg mL<sup>-1</sup>). (D) Fluorescence spectra of P-probe (1 μM) with increasing 2D MoS<sub>2</sub> (0–12.3 μg mL<sup>-1</sup>; interval: 1.2 μg mL<sup>-1</sup>). (E) Fluorescence spectra of 2D probe (P-probe/2D MoS<sub>2</sub> = 1 μM/5 μg mL<sup>-1</sup>) with increasing GPC-3 (0–0.3 μM; interval: 0.03 μM). (F) Fluorescence change (where I<sub>0</sub> and I are the fluorescence intensity of 2D probe in the absence and presence of an analyte, respectively) of 2D probe (P-probe/2D MoS<sub>2</sub> = 1 μM/5 μg mL<sup>-1</sup>) with GPC-3 (0.3 μM) or control analytes (from left to right: 1 μM of proteins including human serum albumin, bovine serum albumin, pepsin, immunoglobulin G, lysozyme, and 7.5 μM of ions including Na<sup>+</sup>, K<sup>+</sup>, Ca<sup>2+</sup>, Fe<sup>3+</sup>, Mg<sup>2+</sup>, I<sup>-</sup>, Br<sup>-</sup>, CO<sub>3</sub><sup>2-</sup>, HCO<sub>3</sub><sup>-</sup>, HSO<sub>4</sub><sup>-</sup>, H<sub>2</sub>PO<sub>4</sub><sup>-</sup>). All fluorescence spectra were measured in phosphate buffered saline (0.01 M, pH 7.4) with excitation at 510 nm.

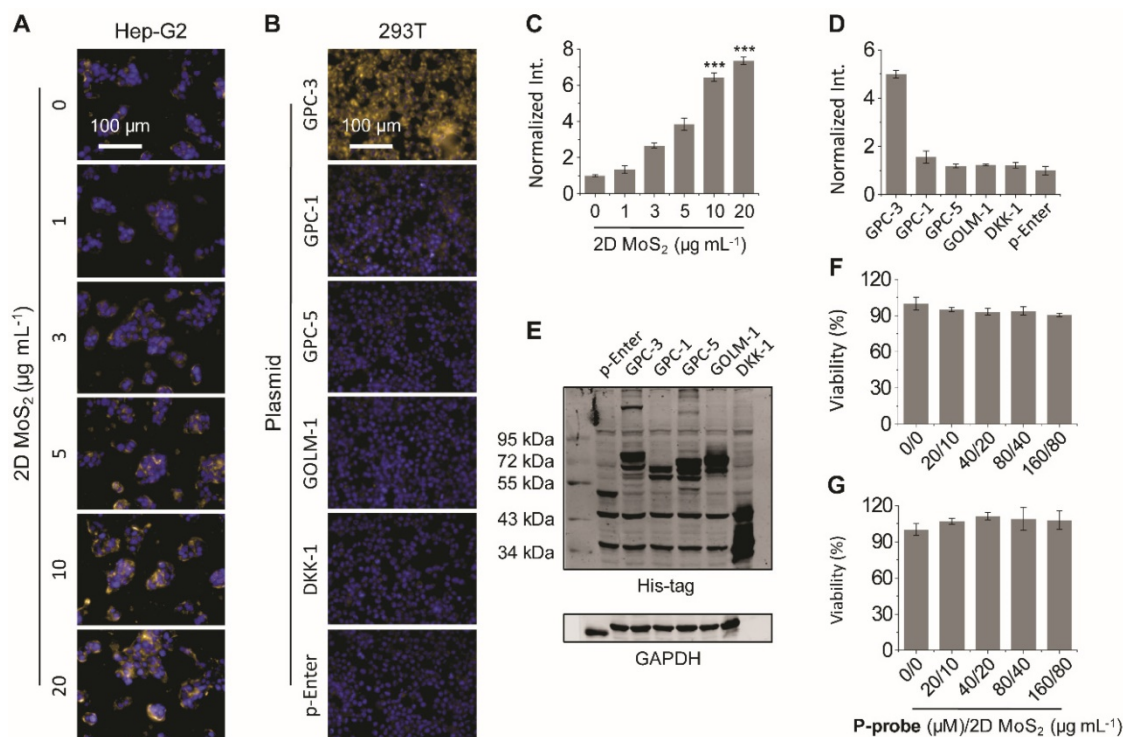


**Figure 3.** Fluorescence imaging (A) and quantification (C) of Hep-G2 (human hepatoma) cells in the presence of P-probe (20 μM) with increasing 2D MoS<sub>2</sub> (\*\*\*P < 0.001 with respect to P-probe alone). Fluorescence imaging (B) and quantification (D) of HEK293T (human embryonic kidney) cells overexpressing different membrane proteins including glypican-3 (GPC-3), glypican-1 (GPC-1), glypican-5 (GPC-5), golgi membrane protein-1 (GOLM-1) and dickkopf-like-1 protein (DKK-1) in the presence of 2D probe (P-probe/2D MoS<sub>2</sub> = 20 μM/10 μg mL<sup>-1</sup>) (p-Enter is the empty plasmid). (E) Western blot analysis of the expression level of different membrane proteins including GPC-3, GPC-1, GPC-5, GOLM-1 and DKK-1 in HEK293T cells after transfection. Viability of (F) Hep-G2 and (G) L02 (human liver) cells in the presence of increasing concentrations of P-probe and 2D MoS<sub>2</sub>. All fluorescence images were recorded using an Operetta high-content imaging system (Perkinelmer, US) (excitation and emission channels used were 520–550 and 580–650 nm, respectively; cell nuclei were stained by Hoechst 33342), and quantified and plotted by Columbus analysis system (Perkinelmer, US).

We observed that the fluorescence of the 2D probe produced in the HCC cell line (Hep-G2) was much larger than that in the normal cell line (L02) (**Figure S2A-B**), and the difference in fluorescence intensity was similar to that of the GPC-3 expression level of the two cell lines as determined by real-time quantitative polymerase chain reaction (**Figure S2C**). This preliminarily verifies the HCC selectivity of the developed 2D probe.

To further corroborate that the imaging is based on the recognition between 2D probe and GPC-3 rather than other proteins that are overexpressed in HCC or structurally close to GPC3, a transfection assay was carried out. GPC-3 and a range of other proteins expressed in HCC cells (including glypican-1 [GPC-1], glypican-5 [GPC-5], golgi membrane protein-1 [GOLM-1] and dickkopf-like-1 protein [DKK-1]) were over-expressed in a human embryonic kidney cell line (HEK293T) through the transfection assay. The expression level of the proteins in HEK293T was determined to be similar using western blotting (**Figure 3E**). Then, the cells were imaged by the 2D probe. We determined that the fluorescence of the 2D probe was only produced in the HEK293T cells that overexpress GPC-3 rather than the control cells expressing other proteins (**Figure 3B, D**), suggesting the good selectivity of the probe for GPC-3. In addition, we observed that the pre-incubation of a free GPC-3 ligand (KKKRLNVGGTYFLTRQ) with Hep-G2 largely suppressed the fluorescence of the 2D probe (**Figure S3**), which also suggests that the imaging is based on the selective interaction between P-probe and GPC-3. The 2D probe was also shown to hardly interrupt the proliferation of Hep-G2 (**Figure 3F**), L02 (**Figure 3G**), and HEK293T cells without transfection and those with an overexpressed GPC-3 level (**Figure S4**).

### GPC-3-targeted imaging of HCC sections

With the promising imaging results obtained at the cellular level, we finally turned our attention to the examination of the diagnostic potential of the 2D probe for clinical tissue sections. Freshly prepared frozen sections removed from patients pathologically confirmed as HCC were used. We first used an HCC-positive section to optimize the incubation time of the 2D probe. It was determined that the probe's fluorescence became appreciable using fluorescence microscope only 1 min after incubation, and the fluorescence reached equilibrium in about 5 min (**Figure 4A**). This suggests the ability of the 2D probe to rapidly diagnose HCC-positive tissues.

We also compared the imaging effect of the 2D probe with that of P-probe alone by time-dependent fluorescence imaging. We determined that while the

P-probe produced an insufficient level of fluorescence on the HCC tissue slide after 15 min of incubation, the use of the 2D probe gave rise to a 6-fold enhanced fluorescence (with respect to the control slide without treatment of probes) (**Figure S5**). This is in agreement with the imaging result at the cellular level, highlighting the ability of 2D MoS<sub>2</sub> to remarkably enhance the binding of the peptide probe with GPC-3 on HCC tissues. To further test the specificity of the probe, we used different tumor and para-carcinoma sections for the imaging experiment. The result showed that whereas all the tumor sections were clearly imaged by the 2D probe (**Figure 4B**), almost no fluorescence was produced in the non-tumor slides (**Figure 4C**).

Subsequently, the imaging precision of 2D probe was compared with traditionally used clinical staining methods (i.e., nuclei staining with Hoechst 33342 and the Hematoxylin-Eosin (H&E) staining; **Figure 4D**) in a double-blind manner. We determined that the fluorescently imaged area of HCC tumor sections (nos. 194260 and 193933) were in accordance with both Hoechst 33342 (the cell nuclei of HCC cells are larger than those of healthy cells) and H&E staining, whereas two control slides (cavernous hemangioma, nos. 192513 and 192544) were not falsely imaged by the probe. This implies the good specificity of the imaging probe for HCC over benign liver tumors. Interestingly, the subsequent fluorescence imaging using two independent frozen sections (nos. 194665 and 194404) containing both HCC-positive and para-carcinoma regions gave rise to the evident differentiation of the two regions (as divided by the dashed curve) (**Figure 4D**). The result is in good accordance with the reference staining methods (Hoechst 33342 and H&E staining). These data clearly suggest the effectiveness of the developed 2D probe facilitating the clinical diagnosis of HCC on frozen sections during surgery.

In order to obtain a cut-off value of the imaging method developed, we used six additional frozen sections containing both cancer and para-carcinoma regions. The sections were treated with the 2D probe, and the fluorescence intensities of the HCC-positive and para-carcinoma (negative) regions, as differentiated by H&E staining (**Figure S6A**), were quantified. Notably, the fluorescence quantification from a single tissue section containing both cancer and para-carcinoma tissues might be more accurate than that from pure positive and negative tissues separately because artificial errors during section preparation and staining could be avoided. On the basis of the statistical relative fluorescence intensity, the positive diagnostic result (gold standard) and the sample size, an ROC curve was drawn. Then, the

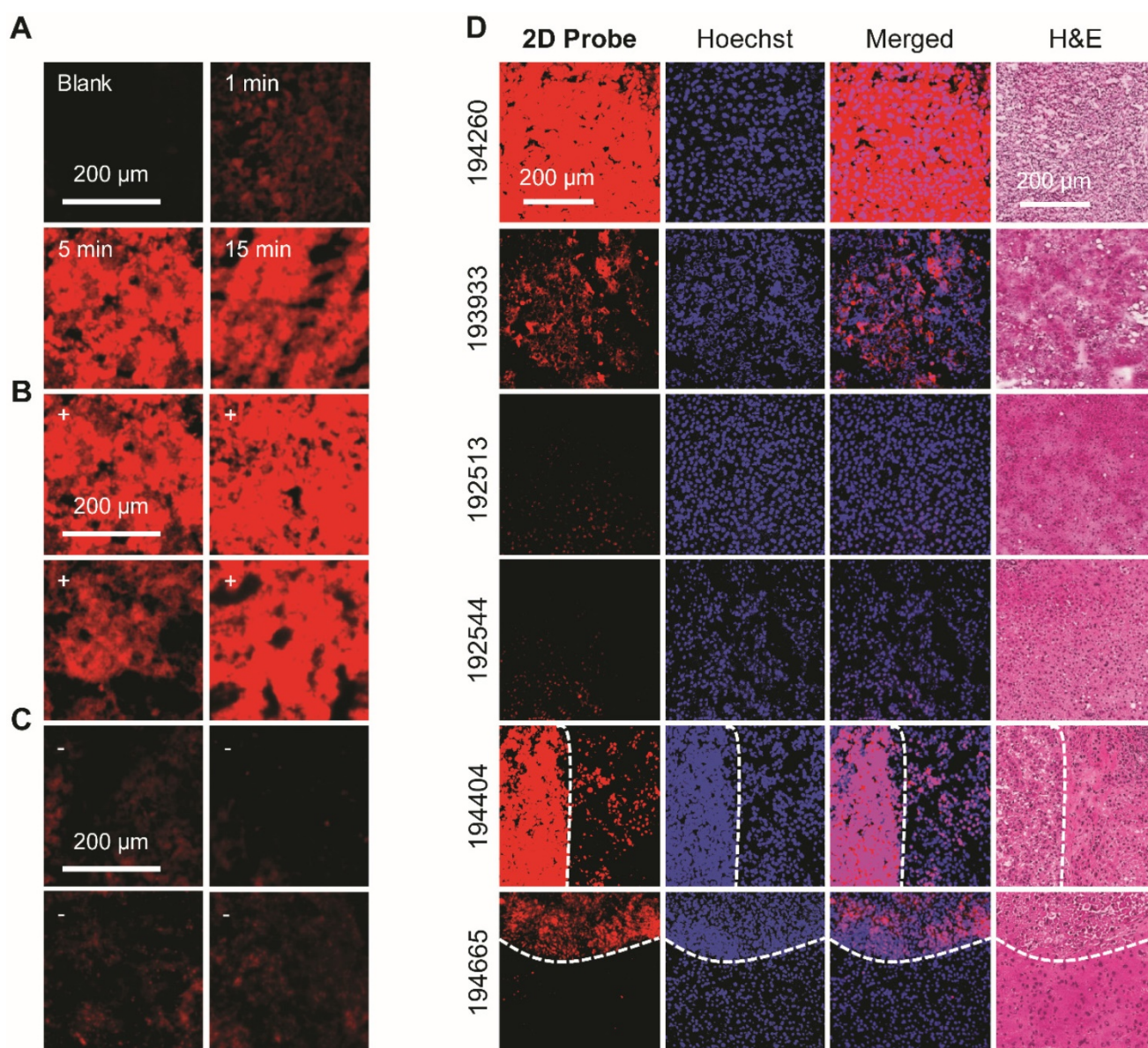


**Figure 4.** (A) Fluorescence imaging of frozen tissue sections removed from HCC patients in the presence of 2D probe (P-probe/2D MoS<sub>2</sub> = 40 μM/20 μg mL<sup>-1</sup>) with time. (B) Fluorescence imaging of four independent frozen tissue slides of HCC after incubation with 2D probe for 5 min. (C) Fluorescence imaging of four independent frozen tissue sections of para-carcinoma after incubation with 2D probe for 5 min. (D) Double-blind fluorescence imaging of different kinds of frozen tissue sections with 2D probe for 5 min (the dashed curves divide HCC-positive from para-carcinoma regions). Hoechst 33342 and H&E (hematoxylin-eosin) staining were used as reference methods. The fluorescence images in (A-C) were obtained on a fluorescence microscope (Olympus, Japan; excitation and emission channels used were 535-555 and 570-625 nm, respectively) and those in (D) on a confocal laser scanning microscope (Olympus, Japan; excitation and emission channels used were 512 and 570-590 nm, respectively).

cut-off value, which is the coordinate closest to the upper left corner of the ROC curve that effectively differentiates the fluorescence intensity of para-carcinoma from that of HCC-positive tissues, was obtained (Figure S6B) [33].

## Conclusion

We have developed a simple 2D imaging probe based on the supramolecular assembly between a fluorescent peptide ligand for GPC-3 and 2D MoS<sub>2</sub>. The probe with minimal background fluorescence and high binding affinity for GPC-3 has been shown to be capable of sensitively and selectively imaging HCC cells and a normal cell line overexpressing GPC-3. We

have also demonstrated the applicability of the 2D probe for the effective imaging of frozen sections removed from HCC patients in a rapid and precise manner. The fact that it can effectively differentiate between HCC-positive and para-carcinoma tissue regions on a single pathological section makes the 2D probe also potentially applicable for fluorescence imaging-guided surgery. We believe that this research offers new insights into the precise and effective clinical diagnosis of HCC using simple and economic supramolecular 2D imaging probes.

## Abbreviations

GPC-3: glypican-3; HCC: hepatocellular

carcinoma; H&E: hematoxylin-eosin; ROC curve: receiver operating characteristic curve; 5-TAMRA: 5-carboxytetramethylrhodamine.

## Supplementary Material

Additional figures including atomic force microscopy images, cell viability and additional cell and tissue imaging results, and the complete Methods section are provided in the Supplementary material associated with this article. Supplementary figures. <http://www.thno.org/v08p3268s1.pdf>

## Acknowledgements

The authors warmly thank the Natural Science Foundation of China (nos. 21788102, 21722801), the State Key Science and Technology Project (no. 2018ZX10732202), the State Key Project for Liver Cancer (no. 2017ZX10203206), the National Key Research and Development Program (nos. 2017YFC0906900 and 2016YFC0902402), the Precision Medicine Project of Second Military Medical University (no. 2017JZ30) and the Shanghai Rising-Star Program (no. 16QA1401400) (to X.-P. He) for generous financial support.

## Competing Interests

The authors have declared that no competing interest exists.

## References

1. Ferenci P, Fried M, Labrecque D, Bruix J, Sherman M, Omata M, et al.; World Gastroenterology Organization. Hepatocellular carcinoma (HCC): a global perspective. *J Clin Gastroenterol.* 2010; 44: 239-45.
2. Zheng J, Kuk D, Gönen M, Balachandran VP, Kingham TP, Allen PJ, et al. Actual 10-year survivors after resection of hepatocellular carcinoma. *Ann Surg Oncol.* 2017; 24: 1358-66.
3. Pilia G, Hughes-Benzie RM, MacKenzie A, Baybayan P, Chen EY, Huber R, et al. Mutations in GPC3, a glypican gene, cause the Simpson-Golabi-Behmel overgrowth syndrome. *Nat Genet.* 1996; 12: 241-7.
4. Hsu HC, Cheng W, Lai PL. Cloning and expression of a developmentally regulated transcript MXR7 in hepatocellular carcinoma: biological significance and temporospatial distribution. *Cancer Res.* 1997; 57: 5179-84.
5. Capurro M, Wanless IR, Sherman M, Deboer G, Shi W, Miyoshi E, et al. Glypican-3: a novel serum and histochemical marker for hepatocellular carcinoma. *Gastroenterology.* 2003; 125: 89-97.
6. Geim AK, Novoselov KS. The rise of graphene. *Nat Mater.* 2007; 6: 183-91.
7. Gupta A, Sakthivel T, Seal S. Recent development in 2D materials beyond graphene. *Prog Mater Sci.* 2015; 73: 44-126.
8. Georgakilas V, Tiwari JN, Kemp KC, Perman JA, Bourlino AB, Kim KS, et al. Noncovalent functionalization of graphene and graphene oxide for energy materials, biosensing, catalytic, and biomedical applications. *Chem Rev.* 2016; 116: 5464-519.
9. Manzeli S, Ovchinnikov D, Pasquier D, Yazyev OV, Kis A. 2D transition metal dichalcogenides. *Nat Rev Mater.* 2017; 2: 17033.
10. Chen Y, Tan C, Zhang H, Wang L. Two-dimensional graphene analogues for biomedical applications. *Chem Soc Rev.* 2015; 44: 2681-701.
11. He XP, Zang Y, James TD, Li J, Chen GR. Probing disease-related proteins with fluorogenic composite materials. *Chem Soc Rev.* 2015; 44: 4239-48.
12. He XP, Hu XL, James TD, Yoon J, Tian H. Multiplexed photoluminescent sensors: towards improved disease diagnostics. *Chem Soc Rev.* 2017; 46: 6687-96.
13. He XP, Tian H. Photoluminescence architectures for disease diagnosis: from graphene to thin-layer transition metal dichalcogenides and oxides. *Small.* 2016; 12: 144-60.
14. Kurapati R, Kostarelos K, Prato M, Bianco A. Biomedical uses for 2D materials beyond graphene: current advances and challenges ahead. *Adv Mater.* 2016; 28: 6052-74.
15. Zhang P, Fu C, Ran W, Meng J, Yin Q, Li Y. Recent progress in light-triggered nanotheranostics for cancer treatment. *Theranostics.* 2016; 6: 948-68.
16. Wang S, Lin J, Wang T, Chen X, Huang P. Recent advances in photoacoustic imaging for deep-tissue biomedical applications. *Theranostics.* 2016; 6: 2394-413.
17. Liu T, Chao Y, Gao M, Liang C, Chen Q, Song G, et al. Ultra-small MoS<sub>2</sub> nanodots with rapid body clearance for photothermal cancer therapy. *Nano Res.* 2016; 8: 22106-12.
18. Hao J, Song G, Liu T, Yi X, Yang K, Cheng L, et al. In vivo long-term biodistribution, excretion, and toxicology of PEGylated transition-metal dichalcogenides MS<sub>2</sub> (M = Mo, W, Ti) nanosheets. *Adv Sci.* 2017; 4: 1600160.
19. Yin W, Yan L, Yu J, Tian G, Zhou L, Zheng X, et al. High-throughput synthesis of single-layer MoS<sub>2</sub> nanosheets as a near-infrared photothermal-triggered drug delivery for effective cancer therapy. *ACS Nano.* 2014; 8: 6922-33.
20. Zhu C, Zeng Z, Li H, Li F, Fan C, Zhang H. Single-layer MoS<sub>2</sub>-based nanopores for homogeneous detection of biomolecules. *J Am Chem Soc.* 2013; 135: 5998-6001.
21. Ji DK, Zhang Y, Zang Y, Li J, Chen GR, He XP, et al. Targeted intracellular production of reactive oxygen species by a 2D molybdenum disulfide glycosheet. *Adv Mater.* 2016; 28: 9356-63.
22. Xie D, Ji DK, Zhang Y, Cao J, Zheng H, Liu L, et al. Targeted fluorescence imaging enhanced by 2D materials: a comparison between 2D MoS<sub>2</sub> and graphene oxide. *Chem Commun.* 2016; 52: 9418-21.
23. Wahiba M, Feng XQ, Zang Y, James TD, Li J, Chen GR, et al. A supramolecular pyrenyl glycoside-coated 2D MoS<sub>2</sub> composite electrode for selective cell capture. *Chem Commun.* 2016; 52: 11689--92.
24. Dou WT, Kong Y, He XP, Chen GR, Zang Y, Li J, et al. GPCR activation and endocytosis induced by a 2D material agonist. *ACS Appl Mater Interfaces.* 2017; 9: 14709-15.
25. Song JX, Tang XY, Zhou DM, Zhang W, James TD, He XP, et al. A fluorogenic 2D glycosheet for the simultaneous identification of human- and avian-receptor specificity in influenza viruses. *Mater Horiz.* 2017; 4: 431-6.
26. Guo S, Chen J, Cai BY, Chen WW, Li YF, Sun X, et al. Low-dimensional materials facilitate the conjugation between fluorogenic boronic acids and saccharides. *Mater Chem Front.* 2017; 1: 61-4.
27. Ma YH, Dou WT, Pan YF, Dong LW, Tan YX, He XP, et al. Fluorogenic 2D peptidosheet unravels CD47 as a potential biomarker for profiling hepatocellular carcinoma and cholangiocarcinoma tissues. *Adv Mater.* 2017; 29: 1604253.
28. Zhu S, Gong L, Xie J, Gu Z, Zhao Y. Design, synthesis, and surface modification of materials based on transition-metal dichalcogenides for biomedical applications. *Small Methods.* 2017; 1: 1700220.
29. Lee LL, Ahn BC, Lee Y, Lee SW, Cho JY, Lee J. Targeting of hepatocellular carcinoma with glypican-3-targeting peptide ligand. *J Pept Sci.* 2011; 17: 763-9.
30. Li J, Du X, Hashim S, Shy A, Xu B. Aromatic-aromatic interactions enable  $\alpha$ -helix to  $\beta$ -sheet transition of peptides to form supramolecular hydrogels. *J Am Chem Soc.* 2017; 139: 71-4.
31. Zhou W, Yin Z, Du Y, Huang X, Zeng Z, Fan Z, et al. Synthesis of few-layer MoS<sub>2</sub> nanosheet-coated TiO<sub>2</sub> nanobelt heterostructures for enhanced photocatalytic activities. *Small.* 2013; 9: 140-7.
32. Loan PTK, Zhang W, Lin CT, Wei KH, Li LJ, Chen CH. Graphene/MoS<sub>2</sub> heterostructures for ultrasensitive detection of DNA hybridisation. *Adv Mater.* 2014; 26: 4838-44.
33. Habibzadeh F, Habibzadeh P, Yadollahie M. On determining the most appropriate test cut-off value: the case of tests with continuous results. *Biochem Medica.* 2016; 26: 297-307.